Ceramics International xxx (xxxx) xxx

Contents lists available at ScienceDirect

Ceramics International

journal homepage: www.elsevier.com/locate/ceramint

Influence of precursor deficiency sites for borate incorporation on the structural and biological properties of boronated hydroxyapatite

Ozkan Gokcekaya [a,b], Celaletdin Ergun [c,*], Thomas J. Webster [d,e,f], Takayoshi Nakano [a,b]

[a] Graduate School of Engineering, Division of Materials and Manufacturing Science, Osaka University, 565-0871, Suita, Osaka, Japan
[b] Anisotropic Design & Additive Manufacturing Research Center, Osaka University, 2-1, Yamadaoka, Suita, Osaka, 565-0871, Japan
[c] Faculty of Mechanical Engineering, Istanbul Technical University, 34437, Istanbul, Turkey
[d] School of Health Sciences and Biomedical Engineering, Hebei University of Technology, Tianjin, 065000, China
[e] Programa de Pós-Graduação em Ciência e Engenharia dos Materiais, Universidade Federal do Piauí, Teresina, 64049-550, Brazil
[f] School of Engineering, Saveetha University, Chennai, 602117, India

ARTICLE INFO

Keywords:
Hydroxyapatite
Chemical synthesis
Borate
Incorporation
Osteoblast adhesion
Osteoblast spreading

ABSTRACT

The biological properties of hydroxyapatite (HA) are significantly influenced by its compositional characteristics especially doping elements and/or Ca/P ratio, which can be altered by precursor chemistry. In this study, a group of boronated (B-incorporated) hydroxyapatite (BHA) was synthesized using a precipitation method by setting the Ca/P ratio to the stoichiometric value of HA (1.67), while altering the precursor chemistry by adjusting either (Ca + B)/P (Ca-deficient precursor, BC) or Ca/(P + B) (P-deficient precursor, BP). After heat-treatment, the partial decomposition of the BC was observed, forming tricalcium phosphate as the byproduct, however, the BP showed phase stability at all temperatures. The B-ionic species in the form of $(BO_2)^-$ and $(BO_3)^{3-}$ were incorporated into the HA structure at the $(PO_4)^{3-}$ and $(OH)^-$ positions, respectively. The incorporation of the B species also facilitated the incorporation of $(CO_3)^{2-}$ groups specifically in the BPs. This is the first finding on BHA reporting that preferential $(CO_3)^{2-}$ incorporation depends on the precursor chemistry used. As a result, osteoblast adhesion was superior on the BPs compared to pure HA owing to the carbonated structure, increasing cell spreading area. As such, this *in vitro* study highlighted that the present P-deficient precursor approach for synthesizing BHA improved biocompatibility properties and should, thus, be further considered for the next-generation of improved orthopedic applications.

1. Introduction

The composition and structure of synthetic hydroxyapatite (HA, $Ca_{10}(PO_4)_6(OH)_2$) resembles that of biological apatite. Due to its ability to form a strong bond with neighboring natural bone, synthetic HA is known for its excellent osteoconductive properties and it is widely used as an implant material and a bone substitute [1–8]. However, biological HA differs from synthetic HA particularly due to its inherent Ca^{2+} and OH^- deficiency [2], mainly caused by the presence of various impurities in its structure, such as carbonates and fluorides.

Attempts have been made to modify HA properties by utilizing the high flexibility of the apatite structure and incorporating ions at both the cation (Ca^{2+}) and anion (PO_4^{3-} and OH^-) sites in its structure [3,9]. The incorporation of many divalent cations (Mg^{2+}, Zn^{2+}, etc.) at the Ca^{2+} site can cause an expansion or a contraction of the HA unit cell depending on the size difference compared to Ca^{2+} ions [4]. In the case of some divalent ions, the occupancy of the monovalent (Ag^+, Cu^+) or trivalent ions (La^{3+}, Y^{3+}, In^{3+}, Bi^{3+}, etc.) in its structure is still a matter of intense research interest [5,6,10–12].

Boron (B), as a trace element, increases the release of growth factors and cytokines, and thus stimulates the wound healing process *in vivo* [13,14]. In addition, it increases the synthesis of RNA and the turnover rate of the extracellular matrix [15]. Moreover, its release from an implant improves the osteogenic differentiation of mesenchymal stem cells (MSCs) [16,17]. In contrast, a high dose of boric acid (over 1000 ng/ml) can decrease the viability of mouse osteoblasts [18], rat bone marrow MSCs [13], and human bone marrow MSCs [20,21], while a low dose (less than 1 ng/ml) does not change the viability of the cells. These controversial findings in the literature can reflect the poor understanding of the effect of B content in biomaterials and the need for further *in*

* Corresponding author.
E-mail address: ergunce@itu.edu.tr (C. Ergun).

https://doi.org/10.1016/j.ceramint.2022.10.232
Received 16 August 2022; Received in revised form 12 October 2022; Accepted 18 October 2022
Available online 20 October 2022

vivo and *in vitro* investigation [13–21].

In this regard, B-incorporated HA (BHA) was prepared here to modify the inherent properties of HA, benefiting from the contributions provided by the incorporated B ions [21]. In BHA, B ions can be incorporated into the HA lattice in the form of borates (BO_3^{3-}) at phosphate sites (PO_4^{3-}) and oxoborane $(BO_2)^-$ at hydroxide (OH^-) sites [21]. This structural modification can result in a disordered BHA structure, facilitating improved biodegradability and osteoinductivity compared to pure HA and β-tricalcium phosphate (β-TCP) [22]. For instance, the stimulatory effect of BHA on the proliferation and differentiation of pre-osteoblastic cells has also been reported [23]. In another study, the sites of the BO_2^- groups in BHA were used for the recognition of sugar chains to demonstrate lymphocyte activity on the BHA surface [24]. Furthermore, BHA altered the proliferation and osteogenic differentiation of bone cells and human bone marrow MSCs in a dose and time-dependent manner while releasing B ions within the first hour [25].

The precipitation method is a well-established process to synthesize HA nanoparticles with various substitute elements [26]. The physicochemical properties of the as-precipitated HA can be altered by several process parameters, including synthesis temperature, pH of the precursor, and the precursor chemistry in an aqueous medium [27–29]. For the synthesis of substituted HA, the precursor ratios can be adjusted to a target Ca/P ratio while considering the substituted elements. In literature studies, it was commonly found that B ions were preferred to replace Ca ions or P ions by adjusting the precursor deficiency accordingly while keeping the (Ca + B)/P or Ca/(P + B) molar ratios constant, based on the assumption that B would become incorporated into Ca or P positions in the resultant structure, respectively [22,30]. However, there is still a lack of understanding for whether B atoms/ions incorporate into Ca sites or P sites. Since the concentration of the precursor solutions is a major factor affecting the type of the reaction that energetically favors the formation of the resultant phase/s in BHAs, it is reasonable to expect that the final properties of the resultant materials would differ as a result of the differences in the precursor preparation approach [31]. In this regard, some of the inconsistent results in the literature can be explained due to this difference. It should also be emphasized that the deviation of the Ca/P ratio from the stoichiometric proportions of pure HA (~1.67) has a significant influence on the biomedical properties of HA itself, including cell adhesion, sinterability, strength, and solubility in the biological environment [32].

Therefore, to determine the best composition of BHA for optimal or maximal biological and other physical properties, it is necessary to evaluate its biological response in terms of the B content as well as how it is prepared. Such knowledge can be very helpful in precisely tailoring the final properties of BHA and to understand its performance as a bioceramic in real clinical applications.

Thus, this study focused on clarifying the effect of the precursor deficiency obtained via either (Ca + B)/P (Ca deficient precursor, BC) or Ca/(P + B) (P deficient precursor, BP) with 0.25 at%, 1 at%, and 3 at% B addition on phase formation after heat treatment and on osteoblast (bone-forming cells; CRL−11,372) activities on the BHAs.

2. Materials and methods

2.1. Synthesis of the boronated HA

Pure HA and BHAs were synthesized using a modified co-precipitation method [33]. For the synthesis of pure HA, concentrated ammonia (NH_4OH) was used to make pH adjustments to separate solutions of 1 M $Ca(NO_3)_2{\cdot}4H_2O$ (Ca-precursor) and 0.6 M $(NH_4)HPO_4$ (P-precursor) to obtain a pH of 11 [34]. In order to synthesize BHAs, a boron-precursor was prepared by dissolving H_3BO_3 in distilled water.

For pure HA, the $Ca(NO_3)_2{\cdot}4H_2O$ was stirred at room temperature (RT), and after adding $(NH_4)HPO_4$ to the solution, it was stirred for 24 h at RT. For BHA nanoparticles (NPs), a H_3BO_3 solution was added to the $Ca(NO_3)_2{\cdot}4H_2O$ or $(NH_4)HPO_4$ solutions to synthesize the BHA samples. For the BC and BP samples, the (Ca + B)/P and Ca/(P + B) ratios, respectively, were ensured to be 1.67. The abbreviations and molar ratios of the samples of interest in this study are given in Table 1.

The details of the synthesis procedure have been explained in our previous study [33]. Briefly, precipitated nano HA particles were filtered and dried, afterwards, cold-pressed pellets were heat-treated at 500 °C, 700 °C, 900 °C, 1100 °C, and 1300 °C (heating rate of 22 °C/min) for 2 h to investigate the effect of B content and heat-treated temperature on their phase stability, as well as osteoblast adhesion on the pellets.

2.2. Characterization

The morphology of the as-precipitated BHA NPs was characterized by transmission electron microscopy (TEM: JEOL 2010F) under an accelerating voltage of 300 kV.

The phase analysis was performed on the heat-treated pellets by X-ray diffraction (XRD, Philips PW2273/20) with a Cu Kα radiation of 40 kV and 40 mA and at scanning diffraction angles of (2θ) 20° and 50° at a scan rate of 10°/min.

The calculations of the hexagonal lattice parameters and the corresponding unit lattice volumes of the BHA samples were carried out by assuming their space group was $p6_3/m$ [2]. The calculations of unit cell parameters (*a* and *c* axes) were performed by the least squares method (Eq. (1)), while corrections were carried out according to the intercept of the Nelson–Riley plots. The lattice spacing (*d*) was determined according to Bragg's law and (*hk0*) or (*00l*) planes were chosen to calculate the lattice parameters.

$$\frac{1}{d^2} = \frac{4\left(h^2 + hk + k^2\right)}{3a^2} + \frac{l^2}{c^2} \tag{1}$$

The unit cell volume (V) of BHAs was calculated using the relationship described in Eq. (2) [35].

$$V = 2.589a^2c \tag{2}$$

The grain size of the heat-treated pellets was investigated by scanning electron microscopy (SEM, Philips/FEI XL30FEG equipped with EDS) and measured by the lineal intercept technique [36]. The densification factor of the heat-treated pellets was calculated according to Ref. [35] with the following equation:

$$DF = \frac{D - D_g}{D_g} \times 100 \tag{3}$$

where D is the density of the BHAs after heat treatment and Dg is the density of the BHA before heat treatment. The chemical composition of pellets was measured by energy-dispersive X-ray spectroscopy (EDS). The functional groups and the bonds present in the heat-treated conditions were identified by Fourier transform infrared (FTIR, PerkinElmer) spectroscopy. The model of the crystal structure visualized with VESTA [37] was proposed for BC and BP (Table 1), corresponding to the FTIR results.

Table 1
Abbreviations and molar ratios in the corresponding precursors of the BHA samples.

	Abbreviation	Charged molar ratios		
		Ca	P	B
BHAs synthesized from Ca-deficient precursor (BC)	BC0.25	9.975	6	0.025
	BC1	9.9	6	0.1
	BC3	9.7	6	0.3
BHAs synthesized from P-deficient precursor (BP)	BP0.25	10	5.975	0.025
	BP1	10	5.9	0.1
	BP3	10	5.7	0.3

2.3. Osteoblast adhesion and spreading

The biocompatibility of BHAs was evaluated by the adhesion of human osteoblasts (bone-forming cells; CRL-11372; ATCC). Details for the osteoblast culture were reported elsewhere [4]. Heat-treated BHAs were sterilized in an autoclave at 121 °C for 21 min and rinsed with phosphate-buffered saline (PBS) before seeding the osteoblasts at a concentration of 2500 cells/cm^2 onto the samples. The osteoblasts seeded on BHAs were then incubated for 4 h under standard cell culture conditions [4]. After incubation, non-adherent cells were rinsed, and afterwards, adherent cells were fixed, stained, and then counted. The mean cell count was reported as the average number of cells from eight random measurements. Pure HA and borosilicate glass were used as reference materials for osteoblast adhesion.

In addition, pre-osteoblasts were used to estimate osteoblast spreading on the BHA samples compared to pure HA samples. For this test, mouse primary osteoblasts (8000 cells/cm^2) were cultured on the samples under standard conditions. The details of handling mouse primary osteoblasts were mentioned elsewhere [38]. The images of the adherent cells on the samples were recorded using a fluorescence microscope (BZ-X710, Keyence) and the number of adherent cells was calculated, and cell spreading was visualized with image processing software (ImageJ) [39].

2.4. Statistical analysis

All experiments were conducted on five heat-treated samples for each condition. Numerical data were analyzed using Student's *t*-tests. The differences at $p < 0.1$ and $p < 0.05$ were considered statistically significant.

3. Results

3.1. Phase formation and structural defects in the boronated HA

Representative TEM images of the as-precipitated BC and BP NPs are shown in Figs. 1 and 2, respectively. Agglomerated NPs were observed for all BHAs. B-incorporation into HA showed no effect on the shape and size of the as-precipitated NPs or their tendency to aggregate (Figs. 1 and 2), compared to pure HA (Supp. Fig. S1). The sizes of the BHA NPs ranged from 20 nm to 50 nm.

Phase analysis of the BC and BP samples heat-treated at 500 °C, 700 °C, 900 °C, 1100 °C, and 1300 °C are presented in Figs. 3 and 4, respectively. Since the patterns for all of the samples matched closely with the standard pattern of pure HA (ICDD#1-84-1998), it can be concluded that HA was detected as the main phase in all the samples, however, the broad XRD peaks indicated that none of the samples were completely crystallized upon heat-treating at 700 °C. Their crystallization seemed to be completed at 900 °C.

It should be noted that BC0.25 and BC1 exhibited a single HA phase at and above 900 °C. A slight amount of α-TCP formation in the BC3 samples was detected (as shown in Fig. 3(c)) indicating that HA thermally decomposed to α-TCP; a similar phenomenon was detected for pure HA (Supp. Fig. S2). At a heat treatment temperature of 1100 °C, BC3 exhibited further thermal decomposition with an increase in the amount of α-TCP phase associated with a newly formed β-TCP phase, both as secondary phases. The HA remained the major phase at 1300 °C, however, a decrease in the amount of both α-TCP and β-TCP phases was observed.

Unlike BC3, the thermal decomposition of the HA phase was not observed in the other BC and BP samples, which all remained thermally stable at all temperatures. The absence of any detectable secondary phases associated with B and/or other calcium phosphate phases suggests that B incorporation took place only by its integration into the solid solution of the HA structure upon heat treatment. The crystallization of the BHAs heat-treated at 1100 °C was confirmed by the diffraction patterns taken with TEM (Supp. Fig. S3).

The measured atomic concentrations of B, Ca, and P species and the corresponding Ca/P ratios in the BHA samples heat-treated at 1100 °C based on the SEM-EDS data are shown in Table 2. As expected, the B concentration increased in all the samples with increasing B content in the precursor solutions. The concentration of B ions was higher in BP than in BC. On one hand, the measured Ca/P ratio in the BC samples increased as the Ca/P ratio decreased in the precursor solution, indicating that not all of the PO_4^{3-} ions were included in the reaction to form HA. On the other hand, the measured Ca/P ratio in the BP samples first slightly increased in BP0.25 and BP1, and then decreased showing a similar Ca/P ratio with the charged value, thus indicating an efficient HA synthesis reaction in terms of Ca and P source use for BP3 (Table 2). Accordingly, it can be generalized that the Ca/P ratio in the BC samples may have an increasing tendency with greater B concentrations. However, it may be assumed that the Ca/P ratio in the BP samples may have a decreasing tendency with further increasing B concentrations.

The calculations of the hexagonal lattice parameters and the differences in the corresponding unit lattice volumes of the BHA samples heat-treated at 1100 °C are given in Table 2. The results showed that the BHA lattice volumes expanded upon B incorporation as shown by the increase in lattice volume (Supp. Table S1).

The FTIR spectra of the BHA heat-treated at 1100 °C showed a systematic change in hydroxyl, carbonate, and borate bands with increasing B content (Fig. 5), given in detail in Table 3. The strong bands in the range of 900–1200 cm^{-1} correspond to the P–O stretching vibration modes of phosphate groups, similar to those in the pure HA (Supp. Fig. S4). On the other hand, the bands in the range of 743–782 cm^{-1} can be assigned to the antisymmetric stretching and 1206–1312 cm^{-1} to the symmetric bending of the BO_3^{3-} groups observed

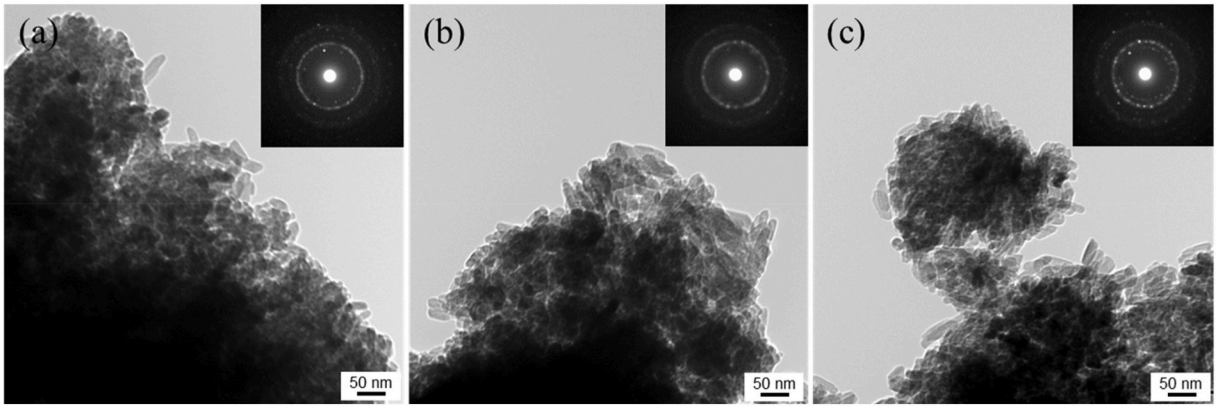

Fig. 1. TEM images of the as-precipitated BC NPs: (a) BC0.25, (b) BC1, and (c) BC3.

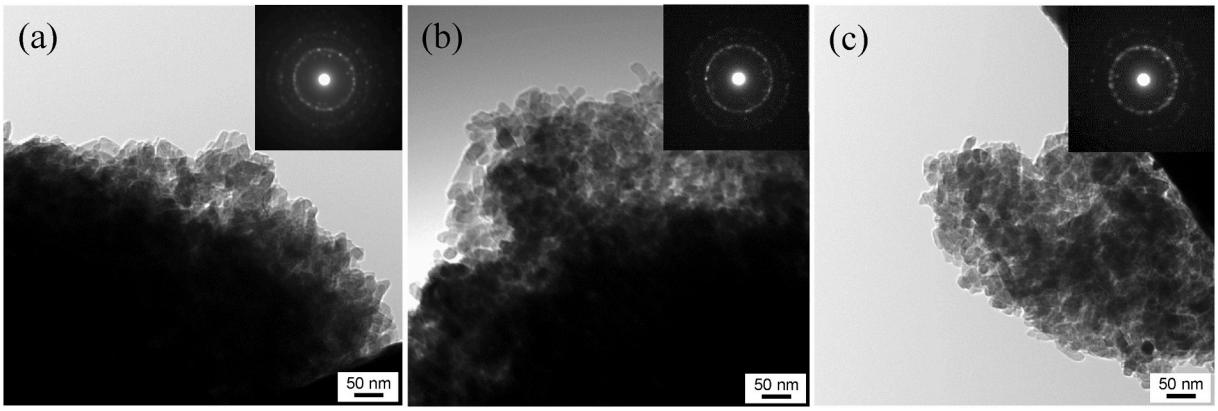

Fig. 2. TEM images of the as-precipitated BP NPs: (a) BP0.25, (b) BP1, and (c) BP3.

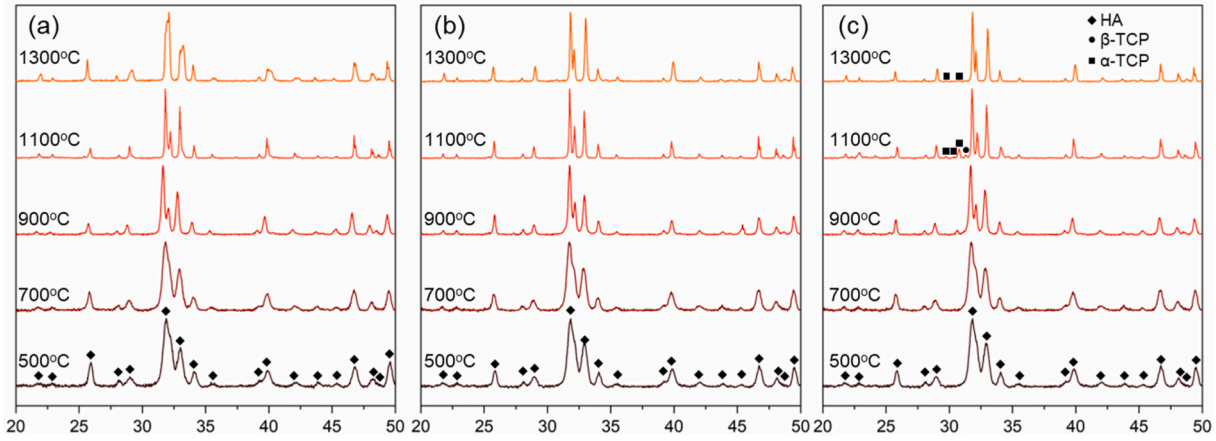

Fig. 3. XRD patterns of the heat-treated BCs: (a) BC0.25, (b) BC1, and (c) BC3. X: axis: 2θ angle, Y-axis: arbitrary units.

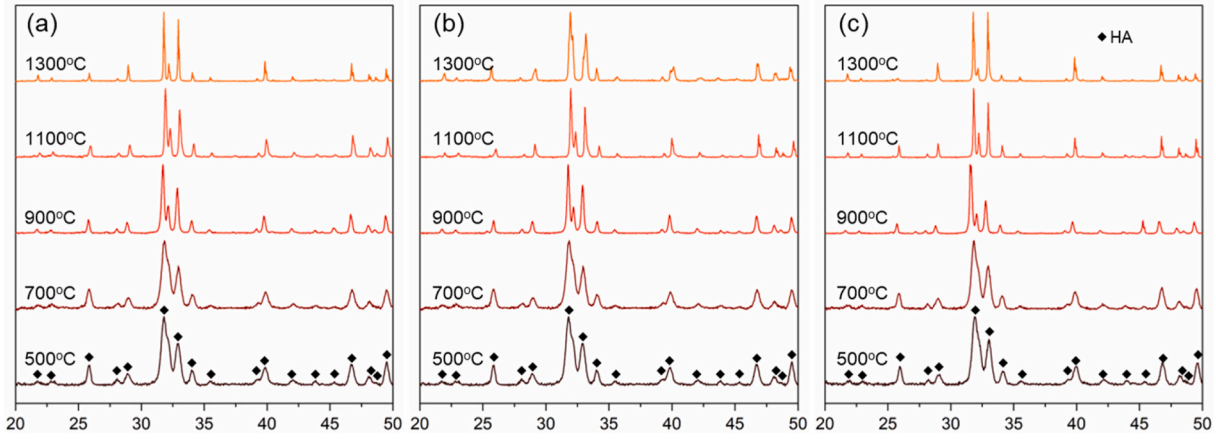

Fig. 4. XRD patterns of the heat-treated BPs: (a) BP0.25, (b) BP1, and (c) BP3. X: axis: 2θ angle, Y-axis: arbitrary units.

particularly in the BHAs, apart from the standard borosilicate glass (Supp. Fig. S4). Furthermore, the pair of weak peaks at 1932 cm^{-1} and 2002 cm^{-1} can be assigned to the antisymmetric stretching of the linear BO_2^- groups [21]. Interestingly, the carbonate bands and asymmetric stretching vibration observed in the range of 1400–1500 cm^{-1} and 885 cm^{-1} (Fig. 5) provided evidence for B-type carbonation in the BP samples with the carbonate (CO_3^{2-}) species provided from the environment during the precipitation process [23].

However, no carbonate stretching band at 1564 cm^{-1} (belonging to the A-type carbonation of the HA structure) was detected. These findings suggest that the BP samples have a B-type carbonated HA structure. It should be noted that the bands related to borate became significant when the B ratios increased. On the other hand, as the borate ratio increased in the BC samples, the intensity of the OH^- stretching band at 3570 cm^{-1} decreased, especially in the case of the BC3 sample.

The results from SEM micrographs (Fig. 6) showed that all BHA samples became highly densified upon heat treatment at 1100 °C. The average grain sizes of the samples are summarized in Table 2. As a

Table 2
Measured composition and corresponding change in the unit volume and average grain size of BHAs heat-treated at 1100 °C.

Sample	Intended Ca/P	Measured atomic ratios			ΔV (nm^3)	Average grain size (μm)
		Ca/P	Change in Ca/P	B at. %		
BC0.25	1.663	1.71	2.83%	0.11	1.684	5.1 ± 0.36
BC1	1.650	1.73	4.85%	0.12	1.229	3.3 ± 0.21
BC3	1.617	1.79	10.70%	0.29	1.337	2.3 ± 0.33
BP0.25	1.674	1.78	6.33%	0.17	1.032	6.9 ± 0.34
BP1	1.695	1.79	5.60%	0.25	0.531	5.9 ± 0.44
BP3	1.754	1.72	−1.94%	0.33	1.684	4.8 ± 0.56

ΔV: The difference in unit lattice volume compared to pure HA

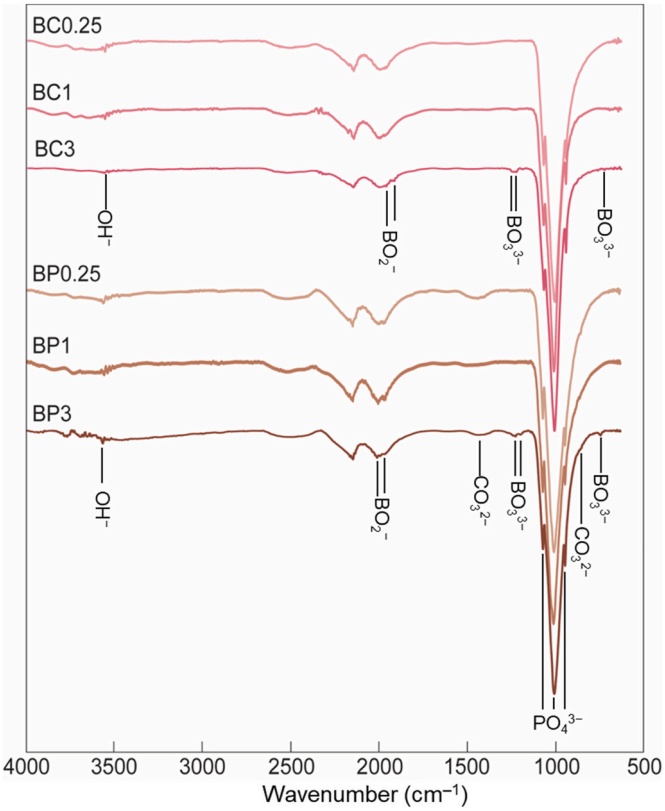

Fig. 5. FTIR spectra for the BC and BP samples heat-treated at 1100 °C. Y-axis: arbitrary units.

general trend, the reduction in the grain size was proportional to the increase in B content for both types of samples, which can be correlated to the change in crystallite size.

3.2. Densification of the boronated HA

The densification factor (DF) of heat-treated BHAs was calculated using Eq. (2) (Fig. 7). The results exhibited that the density of the samples fluctuated up to 900 °C, most probably due to the loss of absorbed and/or structural water and increasing crystallization. The density of the samples showed, in general, an increase with an increasing heat treatment temperature from 700 °C to 1100 °C. The BP0.25 and BP1 exhibited early densification, whereas, BC1 and BC3 densified at a higher temperature range.

In contrast, the density of BC3 was the smallest, particularly at heat treatment temperatures of 900 °C and higher, which can be related to the phase decomposition as indicated with XRD analysis (Fig. 3) and subsequent dehydration of the OH^- groups [40].

3.3. Osteoblast adhesion on the boronated HA

To assess the biocompatibility of the BHA samples, osteoblast (bone-forming cells) adhesion tests were conducted on those samples heat-treated at 1100 °C. The osteoblast adhesion results are presented in Fig. 8(a). The viable osteoblasts on all BHAs tended to be higher in mean value than the pure HA sample, indicating a clear improvement in osteoblast adhesion over pure HA even with a slight amount of B incorporation. Although BC samples presented a progressive increase in osteoblast adhesion at a factor of 1.3–1.6 over pure HA, with an increase in the incorporated B ratio, no statistically significant differences were found between BC samples and pure HA. However, greater osteoblast adhesion behavior on the BP samples was observed by a factor of 2.4–2.85. For instance, the difference in osteoblast adhesion between the BP0.25 and BP3 samples was significant ($p < 0.1$) compared to that of pure HA. Besides, the significant difference between BP1 and pure HA increased ($p < 0.05$), indicating superior biocompatibility.

Fig. 8(b) shows fluorescent images of osteoblasts cultured for 24 h on the pure HA, BC, and BP samples. The amount and the spreading of osteoblasts on the surfaces of pure HA and BC were relatively less. In contrast, the amount and spreading of osteoblasts on the BP samples were greater with a denser network of actin fibers. According to the image processing results, the percentage area covered by osteoblasts adherent to pure HA was about 3.3%. On the other hand, it was 10.8%, 27.6% and 15.3% for 0.25BC, 1BC, and 3BC, respectively. Remarkably, it was the highest at 38.1%, 43.1%, and 36.9% for 0.25BP, 1BP, and 3BP, respectively.

4. Discussion

4.1. Structure of the boronated HA

As emphasized in the literature, the HA structure can form a vast range of solid solutions with a vast variety of cations and anions in the form of simple incorporations into Ca^{2+}, PO_4^{3-}, and/or OH^- positions. Therefore, it can be assumed that the incorporation of cations and/or anions to replace Ca^{2+}, PO_4^{3-}, and/or OH^- ions would change the lattice parameters, depending upon the incorporated ion size.

Furthermore, since the Ca^{2+} ions in the Ca(I) site is less in volume than the ones in the Ca(II) site [41], it is reasonable to assume that a larger cation would occupy the Ca(II) site. However, this generalization is not always true considering the incorporation of a monovalent cation (such as B^+) to divalent Ca^{2+} positions, resulting in an overall charge imbalance. Besides, incorporation of borate ions (BO_3^{3-} and BO_2^-) to

Table 3
Infrared band wavenumbers (cm^{-1}) and assignments for BHAs depending on boron content.

	ν (OH^-)	ν_3 (BO_2^-)	ν_1 (CO_3^{2-})	ν_3 (BO_3^{3-})	ν_1 (PO_4^{3-})	ν_2 (CO_3^{2-})	ν_1 (BO_3^{3-})
BC0.25	3570	2002–1932	–	–	1200–900	–	–
BC1	3570	2002–1932	–	1312	1200–900	–	–
BC3	–	2002–1932	–	1312–1206	1200–900	–	782–743
BP0.25	3570	2002–1932	1545–1454	–	1200–900	878	–
BP1	3570	2002–1932	1545–1454	1312	1200–900	878	–
BP3	3570	2002–1932	1545–1454	1312–1206	1200–900	878	782–743

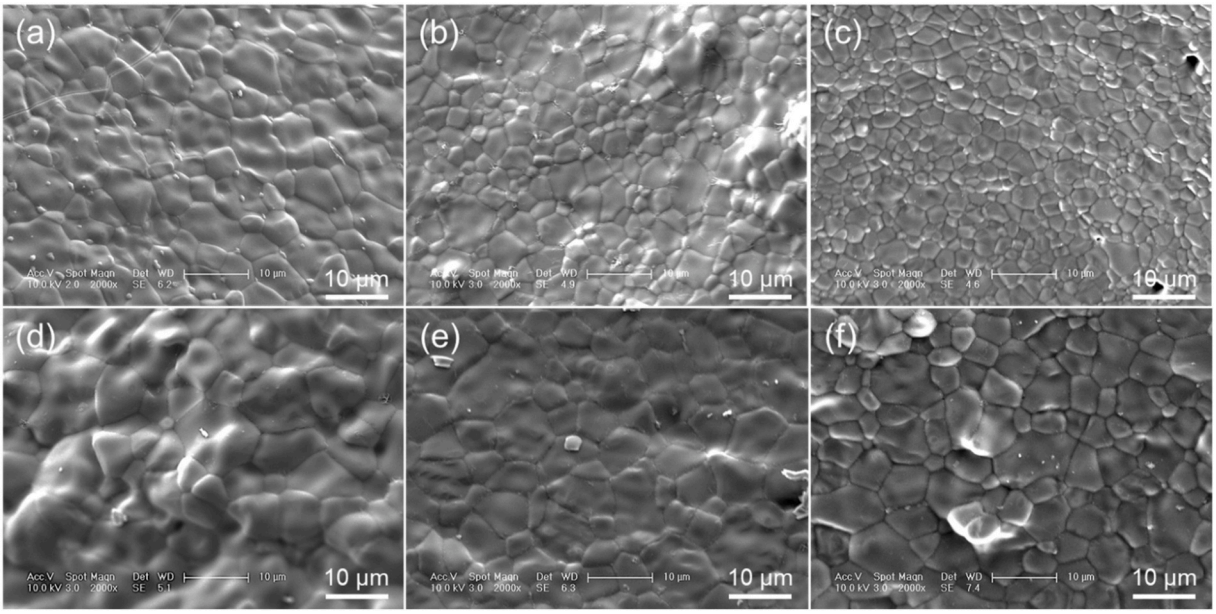

Fig. 6. SEM images of the BHA samples heat-treated at 1100 °C: (a) BC0.25; (b) BC1; (c) BC3; (d) BP0.25; (e) BP1; and (f) BP3.

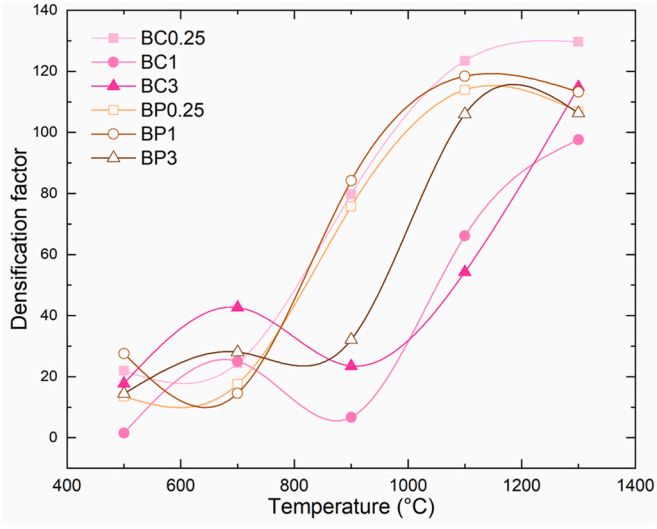

Fig. 7. Densification factors of the BC and BP samples.

PO_4^{3-} and OH^- anion sites have been the main concerns, which was discussed in this study. The charge imbalance in the apatite lattice should be neutralized perhaps by vacancy formation [42], or by multi-ion incorporation to preserve the charge balance of the lattice without vacancy formation [43]. Another possibility is the incorporation of some cations in an interstitial crystallographic site located along the hexagonal channel between two hydroxyl crystallographic sites, possibly facilitated by an OH^- deficiency associated with further O^{2-} incorporation to compensate for any charge imbalance [44].

According to the literature, a shrinkage in the *a*-axis and expansion of the *c*-axis, and the overall increase in lattice volume, occurred upon B incorporation into the HA structure [22]. However, in this study of interest, the lattice parameters (*a*-axis and *c*-axis) were larger than those of pure HA and their distribution (Supp. Table S1) was irregular among the BHA samples. This seems to be most likely due to the multiple possibilities in the preferential incorporation sites for B ions in the HA structure, which is proposed for a future study. For instance, both the BO_3^{3-} and BO_2^- groups were distinctively detected in the BC3 and BP3 samples, respectively, in the FTIR results (Fig. 5), as evidence for B incorporation into the HA lattice, particularly into the PO_4^{3-} sites and the OH^- sites located along the c-axis [21].

On the other hand, the comparison of the FTIR results of the BHA samples revealed that the CO_3^{2-} vibration bands appeared specifically in the BP samples (Fig. 5), while the OH^- vibration bands observed in the BC samples disappeared. It is plausible to expect that the incorporation of monovalent anions, such as BO_2^- groups, into OH^- positions in the anion channel, and trivalent anions, such as BO_3^{3-} groups, into the PO_4^{3-} sites should not cause an overall charge imbalance. However, the incorporation of divalent anions, such as CO_3^{2-} groups, should cause a charge imbalance, and therefore OH^- groups should have been depleted from the structure of the BP samples to preserve the charge balance, and thus the OH^- vibration bands disappeared [44]. It should be emphasized that the additional incorporation of carbonate groups should have further influenced the lattice parameters over B incorporation alone, specifically in the BP samples.

As given in Table 2, as expected, the B concentration in all samples increased with greater B concentrations in their respective precursor solutions. Nevertheless, the concentration of B ions was higher in the BP samples than in their BC counterparts. More interestingly, the Ca/P ratios detected in the BCs were always higher than the Ca/P ratios in the precursor solutions from which they were synthesized. Furthermore, this difference showed a further increase with greater B concentrations. It was assumed that this phenomenon caused the formation of HPO_4^{2-} from unreacted PO_4^{3-} ions although it was undetected from FTIR observations. Thus, this possibly resulted in a low amount of Ca-deficient HA (Ca/P = 1.50) which possessed a high likelihood to decompose into TCP phases as detected from XRD observations. On the other hand, even though the Ca/P ratios were higher in the BP0.25 and BP1 samples than those in the precursor solutions similar to the BC samples, they tended to approach the charged value with an increase of B addition, possibly promoting stable boronated HA formation which exhibited phase stability at high temperatures. Similarly, the difference first increased and suddenly decreased with an increase in B concentration.

These results strongly suggest that the P depletion in the respected samples was most probably due to the incorporation of B-ionic species into the sites occupied by P species. It should also be mentioned that there is no evidence for the occupation of B-ionic species into any Ca^{2+} sites in the HA structure.

In the overall crystal structures of the BC and BP samples, the BO_3^{3-}

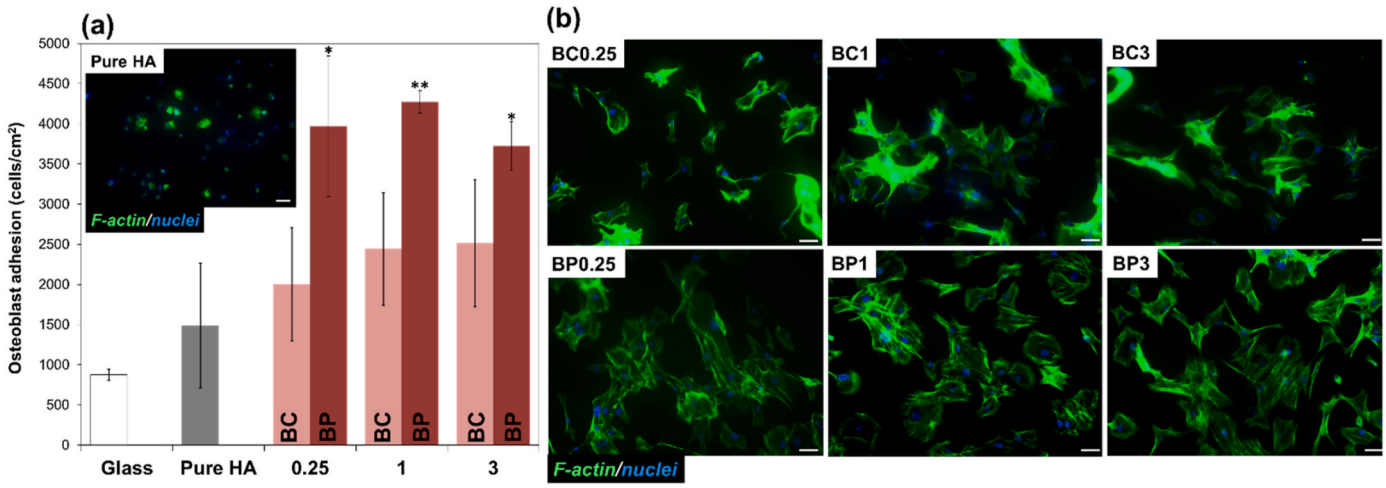

Fig. 8. Analysis of (a) the density of osteoblasts cultured on the BC and BP samples heat-treated at 1100 °C and (b) fluorescent images of osteoblast spreading on the samples after 24 h. The scale bar indicates 50 μm. (*p < 0.1, **p < 0.05 compared to pure HA as the control).

and BO_2^- groups should have been incorporated at the PO_4^{3-} sites and OH^- sites, respectively. Furthermore, the CO_3^{2-} groups should have been incorporated at the PO_4^{3-} positions, specifically in the BP samples.

In this respect, the proposed chemical formulas for the BC and BP samples are as follows:

Ca − deficient BHA

$$Ca_{10}\{(PO_4)_{6-x}(BO_3)_x\}\{(OH)_{2-z}(BO_2)_z\}$$

P − deficient BHA

$$Ca_{10}\{(PO_4)_{6-x-y}(BO_3)_x(CO_3)_y\}\{(OH)_{2-z+y}(BO_2)_z\}$$

Based on these chemical formulas, the proposed models of the unit cells of the BC and BP samples are illustrated in Fig. 9.

In fact, CO_3^{2-} groups can be incorporated into the OH^- sites (the so-called A-type) or PO_4^{3-} sites (the so-called B-type) in the HA structure. Although the A-type becomes energetically more favorable than the B-type in a high-temperature environment, the B-type is more favorable in an aqueous solution environment [45]. In this regard, it can be stated that the BP samples have a B-type CO_3^{2-} incorporation. Extra carbonation of the BP samples also explains why these samples possess better densification behavior at lower temperatures compared to their BC counterparts.

Furthermore, the BHA samples indicated that increasing B addition beyond 0.3% (apparently the solubility limit for the B ions), led to the decomposition of the HA structure, forming α-TCP and β-TCP phases in the BC samples, as presented for BC3 in Fig. 3(c). Interestingly, the decomposition of BC3 into α-TCP was detected at heat treatment temperatures as low as 900 °C, although the decomposition of pure HA to α-TCP normally occurs at about 1270 °C [2]. In this sense, which was also observed for the Ti ions in the Ti incorporated HAs [40], B ions may be considered as an α-TCP stabilizing agent in the HA structure for the BC samples. No decomposition in the HA phase was observed for any BP samples, even heat treatment at 1300 °C (Fig. 4).

4.2. Osteoblast adhesion and spreading on boronated HA

The BC samples enhanced osteoblast adhesion by as much as 60% over pure HA (Fig. 8(a)), although the difference in the osteoblast adhesion was not statistically significant. On the other hand, the enhancement of osteoblast adhesion on the BP samples was remarkable, with an increase of as much as 185% in the case of BP2 samples. It is worth noting that a further increase in borate ion concentration in BP samples (BP3) exhibited a decrease in osteoblast adhesion and spreading properties as shown in Fig. 8. The underlying reasons for the much better

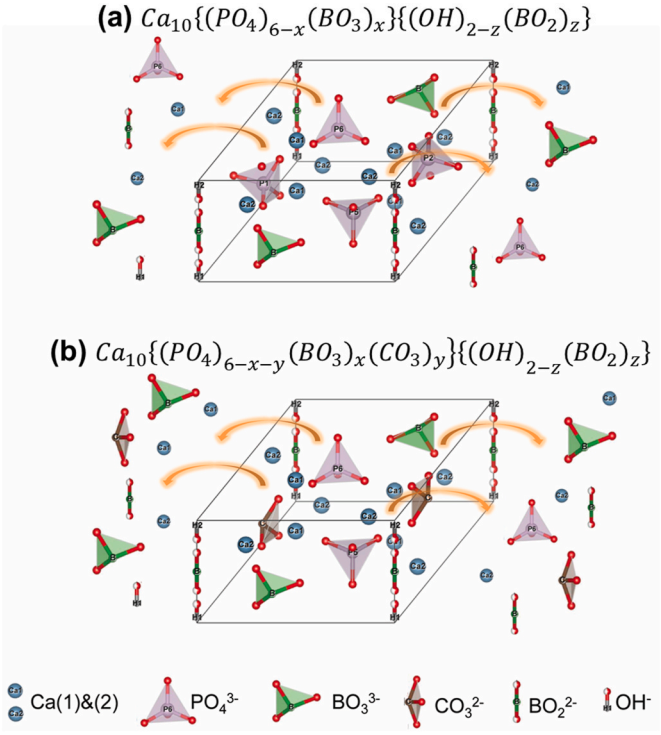

Fig. 9. Representation of BHA structure models and expected ionic species in the biological environment synthesized with (a) Ca-deficient (BC) and (b) P-deficient (BP) precursors.

osteoblast adhesion behavior on BHA than that on pure HA can be attributed to a combination of multiple effects. As expected, the inherent properties of the B species themselves incorporated into the HA structure may have enhanced osteoblast adhesion [45]. Moreover, the morphology of the adherent osteoblasts on the surface of the biomaterials of interest along with their density is strongly correlated with osseointegration and the quality of the regenerated tissue [46]. According to the osteoblast adhesion and spreading assays, the osteoblasts adherent on the BP samples covered a much larger area having a significantly more widespread morphology associated with a dense network of longer actin fibers (Fig. 8(b)).

It should be emphasized that the reason for the 60% better osteoblast adhesion on the BC samples than that on pure HA can be due to B

incorporation into its HA structure. However, the reason for the 120% lower osteoblast adhesion on the BC samples than that on BP samples cannot be addressed only due to the existence of a slight amount of α-TCP and β-TCP as secondary phases in the BC samples, which had a predominant HA phase, since even pure TCP itself had about a 50% lower osteoblast adhesion than pure HA [47]. Indeed, increased proliferation and osteogenic differentiation of bone cells and MSCs with increasing alkaline phosphatase activity was observed on BHA compared to pure HA [25].

In this regard, the reason for the superior osteoblast adhesion on the BP samples can be due to the incorporation of carbonate groups associated with the B-ionic species which, subsequently, may have increased the solubility [48] of the BP samples in an aqueous medium, therefore, increasing the release of the ionic species, including Ca, P, OH, B, etc., as illustrated in Fig. 9, stimulating the maturation of osteoblast focal adhesion to proteins adsorbed on their surfaces [49]. Similar observations were reported for Ag-incorporated HA presenting better antibacterial activity owing to its carbonated structure formed when synthesized from a P-deficient precursor [50]. Additionally, the reduction in grain sizes due to boron incorporation may have altered surface properties (i.e., surface energy, dissolution behavior, etc.), and, thus, this might also contribute to enhanced osteoblast interactions.

The novel results of this study demonstrated that the type of deficiency in the precursor solution (Ca-deficient or P-deficient) and corresponding compensation with the addition of B-precursor had a substantial influence on the amount and the morphology of the osteoblast adhesion on the surface of the boronated HAs. It should be concluded that besides benefiting from the higher biocompatibility provided by B ions, carbonation of the HA structure can easily be carried out by synthesizing it from P-deficient precursors with tailored biological properties.

5. Conclusion

In this study, boronated (B-incorporated) HA NPs synthesized from Ca-deficient or P-deficient precursor solutions with the deficiency site counterbalanced with B-ions at a stoichiometric value of 1.67 were obtained and characterized. The following conclusions summarize the novel findings from this research:

- B-incorporation occurred in the form of BO_3^{3-} ions incorporated into PO_4^{3-} sites and BO_2^- ions were incorporated into OH^- sites in both types of boronated HAs. Moreover, the incorporation of CO_3^{2-} ions into PO_4^{3-} sites can occur specifically in the BHA synthesized from P-deficient precursors.
- A higher amount of B incorporation can occur into the BHAs when synthesized from the P-deficient precursors.
- After heat-treatment, the BC was decomposed to tricalcium phosphate as the byproduct, however, the BP showed a stable HA phase at all temperatures. Both types of BHAs can be highly densified upon heat treatment at 1100 °C.
- In both types of BHAs, the mean value of osteoblast adhesion improved compared to pure HA. Remarkably, the increase in osteoblast adhesion (and associated increased osteoblast spreading with a dense network of actin fibers) on the BHAs synthesized from P-deficient precursors was significant at a factor of 180%.

This investigation demonstrated that a Ca-deficiency or a P-deficiency in the precursor solution has a significant effect on the overall osteoblast adhesion and spreading behavior on BHAs. The osteoblast adhesion behavior on BHA synthesized from P-deficient precursors was shown to be superior to that on pure HA and BHA synthesized from Ca-deficient precursors. These results indicated that the P-deficiency approach in the precursor solution, with its enhanced osteoblast adhesion and cell spreading behavior, has great potential as an alternative for improved bone regeneration and should be further studied.

Declaration of competing interest

The authors declare that they have no known competing financial interests or personal relationships that could have appeared to influence the work reported in this paper.

Acknowledgement

The authors thank Mr. Tadaaki Matsuzaka from Osaka University for his support on the biological analyses. This research was funded by the Scientific and Technological Research Council of Turkey (TUBITAK Contract No: 106M053) and a Grant-in-Aid for Scientific Research (JP18H05254) from the Japan Society for the Promotion of Science (JSPS).

Appendix A. Supplementary data

Supplementary data to this article can be found online at https://doi.org/10.1016/j.ceramint.2022.10.232.

References

[1] M.J. Dalby, L. Di Silvio, E.J. Harper, W. Bonfield, Initial interaction of osteoblasts with the surface of a hydroxyapatite-poly(methylmethacrylate) cement, Biomaterials 22 (2001) 1739–1747, https://doi.org/10.1016/S0142-9612(00)00334-3.
[2] J.C. Elliott, Structure and Chemistry of the Apatites Acnd Other Calcium Orthophosphates, Elsevier Science, 2013.
[3] M. supova, Substituted hydroxyapatites for biomedical applications: a review, Ceram. Int. 41 (2015) 9203–9231, https://doi.org/10.1016/j.ceramint.2015.03.316.
[4] T.J. Webster, E.A. Massa-Schlueter, J.L. Smith, E.B. Slamovich, Osteoblast response to hydroxyapatite doped with divalent and trivalent cations, Biomaterials 25 (2004) 2111–2121, https://doi.org/10.1016/j.biomaterials.2003.09.001.
[5] O. Gokcekaya, K. Ueda, K. Ogasawara, H. Kanetaka, T. Narushima, In vitro evaluation of Ag-containing calcium phosphates: effectiveness of Ag-incorporated β-tricalcium phosphate, Mater. Sci. Eng. C 75 (2017) 926–933, hhttps://doi.org/10.1016/j.msec.2017.02.059.
[6] V. Stanic, S. Dimitrijevic, J. Antic-Stankovic, M. Mitric, B. Jokic, I.B. Plecas, S. Raicevic, Synthesis, characterization and antimicrobial activity of copper and zinc-doped hydroxyapatite nanopowders, Appl. Surf. Sci. 256 (2010) 6083–6089.
[7] O. Gokcekaya, T.J. Webster, K. Ueda, T. Narushima, C. Ergun, In vitro performance of Ag-incorporated hydroxyapatite and its adhesive porous coatings deposited by electrostatic spraying, Mater. Sci. Eng. C 77 (2017) 556–564, https://doi.org/10.1016/j.msec.2017.03.233.
[8] G. Singh, R.P. Singh, S.S. Jolly, Customized hydroxyapatites for bone-tissue engineering and drug delivery applications: a review, J. Sol. Gel Sci. Technol. 94 (2020) 505–530, https://doi.org/10.1007/s10971-020-05222-1.
[9] O. Gokcekaya, K. Ueda, T. Narushima, T. Nakano, Using HAADF-STEM for atomic-scale evaluation of incorporation of antibacterial Ag atoms in a β-tricalcium phosphate structure, Nanoscale 12 (2020) 16596–16604, https://doi.org/10.1039/D0NR04208K.
[10] O. Gokcekaya, K. Ueda, K. Ogasawara, T. Narushima, Antibacterial activity of Ag nanoparticle-containing hydroxyapatite powders in simulated body fluids with Cl ions, Mater. Chem. Phys. 223 (2019) 473–478, https://doi.org/10.1016/j.matchemphys.2018.11.015.
[11] S. Kamonwannasit, C.M. Futalan, P. Khemthong, T. Butburee, A. Karaphun, P. Phatai, Synthesis of copper-silver doped hydroxyapatite via ultrasonic coupled sol-gel techniques: structural and antibacterial studies, J. Sol. Gel Sci. Technol. 96 (2020) 452–463, https://doi.org/10.1007/s10971-020-05407-8.
[12] F. Ai, L. Chen, J. Yan, K. Yang, S. Li, H. Duan, C. Cao, W. Li, K. Zhou, Hydroxyapatite scaffolds containing copper for bone tissue engineering, J. Sol. Gel Sci. Technol. 95 (2020) 168–179, https://doi.org/10.1007/s10971-020-05285-0.
[13] B.-A.-H. Movahedi Najafabadi, M.H. Abnosi, Boron induces early matrix mineralization via calcium deposition and elevation of alkaline phosphatase activity in differentiated rat bone marrow mesenchymal stem cells, Cell J 18 (2016) 62–73, https://doi.org/10.22074/cellj.2016.3988.
[14] A. Dogan, S. Demirci, Y. Bayir, Z. Halici, E. Karakus, A. Aydin, E. Cadirci, A. Albayrak, E. Demirci, A. Karaman, A.K. Ayan, C. Gundogdu, F. sahin, Boron containing poly-(lactide-co-glycolide) (PLGA) scaffolds for bone tissue engineering, Mater. Sci. Eng. C 44 (2014) 246–253, https://doi.org/10.1016/j.msec.2014.08.035.
[15] M. Dzondo-Gadet, R. Mayap-Nzietchueng, K. Hess, P. Nabet, F. Belleville, B. Dousset, Action of boron at the molecular level, Biol. Trace Elem. Res. 85 (2002) 23–33, https://doi.org/10.1385/BTER:85:1:23.
[16] F.H. Nielsen, Update on human health effects of boron, J. Trace Elem. Med. Biol. 28 (2014) 383–387, https://doi.org/10.1016/j.jtemb.2014.06.023.
[17] X. Li, X. Wang, X. Jiang, M. Yamaguchi, A. Ito, Y. Bando, D. Golberg, Boron nitride nanotube-enhanced osteogenic differentiation of mesenchymal stem cells,

J. Biomed. Mater. Res. B Appl. Biomater. 104 (2016) 323–329, https://doi.org/10.1002/jbm.b.33391.
[18] S.S. Hakki, B.S. Bozkurt, E.E. Hakki, Boron regulates mineralized tissue-associated proteins in osteoblasts (MC3T3-E1), J. Trace Elem. Med. Biol. 24 (2010) 243–250, https://doi.org/10.1016/j.jtemb.2010.03.003.
[19] X. Ying, S. Cheng, W. Wang, Z. Lin, Q. Chen, W. Zhang, D. Kou, Y. Shen, X. Cheng, F.A. Rompis, L. Peng, C. zhu Lu, Effect of boron on osteogenic differentiation of human bone marrow stromal cells, Biol. Trace Elem. Res. 144 (2011) 306–315, https://doi.org/10.1007/s12011-011-9094-x.
[20] J. Kolmas, F. Velard, A. Jaguszewska, F. Lemaire, H. Kerdjoudj, S.C. Gangloff, A. Kaflak, Substitution of strontium and boron into hydroxyapatite crystals: effect on physicochemical properties and biocompatibility with human Wharton-Jelly stem cells, Mater. Sci. Eng. C 79 (2017) 638–646, https://doi.org/10.1016/j.msec.2017.05.066.
[21] R. Ternane, M.T. Cohen-Adad, G. Panczer, C. Goutaudier, N. Kbir-Ariguib, M. Trabelsi-Ayedi, P. Florian, D. Massiot, Introduction of boron in hydroxyapatite: synthesis and structural characterization, J. Alloys Compd. 333 (2002) 62–71, https://doi.org/10.1016/S0925-8388(01)01558-4.
[22] S. Barheine, S. Hayakawa, C. Jäger, Y. Shirosaki, A. Osaka, Effect of disordered structure of boron-containing calcium phosphates on their in vitro biodegradability, J. Am. Ceram. Soc. 94 (2011) 2656–2662, https://doi.org/10.1111/j.1551-2916.2011.04400.x.
[23] E.O. Tuncay, T.T. Demirtas, M. Gumusderelioglu, Microwave-induced production of boron-doped HAp (B-HAp) and B-HAp coated composite scaffolds, J. Trace Elem. Med. Biol. 40 (2017) 72–81, https://doi.org/10.1016/j.jtemb.2016.12.005.
[24] Z. Bian, A. Liu, Y. Li, G. Fang, Q. Yao, G. Zhang, Z. Wu, Boronic acid sensors with double recognition sites: a review, Analyst 145 (2020) 719–744, https://doi.org/10.1039/C9AN00741E.
[25] M. Gizer, S. Köse, B. Karaosmanoglu, E.Z. Taskiran, A. Berkkan, M. Timuçin, F. Korkusuz, P. Korkusuz, The effect of boron-containing nano-hydroxyapatite on bone cells, Biol. Trace Elem. Res. 193 (2020) 364–376, https://doi.org/10.1007/s12011-019-01710-w.
[26] K. Ishikawa, E. Garskaite, A. Kareiva, Sol-gel synthesis of calcium phosphate-based biomaterials-A review of environmentally benign, simple, and effective synthesis routes, J. Sol. Gel Sci. Technol. 94 (2020) 551–572, https://doi.org/10.1007/s10971-020-05245-8.
[27] L. Guo, B. Li, C. Zhang, Optimization of process parameters for preparation of hydroxyapatite by the sol-gel method, J. Sol. Gel Sci. Technol. 96 (2020) 247–255, https://doi.org/10.1007/s10971-020-05381-1.
[28] O. Gokcekaya, K. Ueda, T. Narushima, Control of Ag Release from Ag-Containing Calcium Phosphates in Simulated Body Fluid, 2015, https://doi.org/10.1002/9781119190134.ch2.
[29] O. Gokcekaya, K. Ueda, T. Narushima, K. Ogasawara, H. Kanetaka, In vitro properties of Ag-containing calcium phosphates, Ceram. Eng. Sci. Proc. (2017) 87–93, https://doi.org/10.1002/9781119321682.ch10.
[30] M.S. AlHammad, Nanostructure hydroxyapatite based ceramics by sol gel method, J. Alloys Compd. 661 (2016) 251–256, https://doi.org/10.1016/j.jallcom.2015.11.045.
[31] J. Huang, C. Chen, Z. Huang, C. Wu, Y. Cheng, S. Chen, Study on the growth morphology and induction mechanism of strontium hydroxyapatite controlled by anionic and cationic surfactants, J. Alloys Compd. 835 (2020), 155385, https://doi.org/10.1016/j.jallcom.2020.155385.
[32] M. Vallet-Regí, J.M. González-Calbet, Calcium phosphates as substitution of bone tissues, Prog. Solid State Chem. 32 (2004) 1–31, https://doi.org/10.1016/j.progsolidstchem.2004.07.001.
[33] O. Gokcekaya, K. Ueda, T. Narushima, C. Ergun, Synthesis and characterization of Ag-containing calcium phosphates with various Ca/P ratios, Mater. Sci. Eng. C 53 (2015) 111–119, https://doi.org/10.1016/j.msec.2015.04.025.
[34] O. Gokcekaya, K. Ueda, T. Narushima, C. Ergun, Preparation of Ag-doped calcium phosphates, in: 8th pacific rim int. Congr, Adv. Mater. Process. 2013, PRICM 8 (2013).
[35] C. Ergun, T.J. Webster, R. Bizios, R.H. Doremus, Hydroxylapatite with substituted magnesium, zinc, cadmium, and yttrium. I. Structure and microstructure, J. Biomed. Mater. Res. 59 (2002) 305–311.
[36] J.C. Wurst, J.A. Nelson, Lineal intercept technique for measuring grain size in two-phase polycrystalline ceramics, J. Am. Ceram. Soc. 55 (1972) 109, https://doi.org/10.1111/j.1151-2916.1972.tb11224.x.
[37] K. Momma, F. Izumi, VESTA 3 for three-dimensional visualization of crystal, volumetric and morphology data, J. Appl. Crystallogr. 44 (2011) 1272–1276, https://doi.org/10.1107/S0021889811038970.
[38] A. Matsugaki, G. Aramoto, T. Ninomiya, H. Sawada, S. Hata, T. Nakano, Abnormal arrangement of a collagen/apatite extracellular matrix orthogonal to osteoblast alignment is constructed by a nanoscale periodic surface structure, Biomaterials 37 (2015) 134–143, https://doi.org/10.1016/j.biomaterials.2014.10.025.
[39] C.T. Rueden, J. Schindelin, M.C. Hiner, B.E. DeZonia, A.E. Walter, E.T. Arena, K. W. Eliceiri, ImageJ2: ImageJ for the next generation of scientific image data, BMC Bioinf. 18 (2017) 529, https://doi.org/10.1186/s12859-017-1934-z.
[40] C. Ergun, Effect of Ti ion substitution on the structure of hydroxylapatite, J. Eur. Ceram. Soc. 28 (2008) 2137–2149, https://doi.org/10.1016/j.jeurceramsoc.2008.03.007.
[41] M. Jiang, J. Terra, A.M. Rossi, M.A. Morales, E.M. Baggio Saitovitch, D.E. Ellis, Fe2+/Fe3+ substitution in hydroxyapatite: theory and experiment, Phys. Rev. B Condens. Matter 66 (2002) 2241071–22410715.
[42] K. Yoshida, H. Hyuga, N. Kondo, H. Kita, M. Sasaki, M. Mitamura, K. Hashimoto, Y. Toda, Substitution model of monovalent (Li, Na, and K), divalent (Mg), and trivalent (Al) metal ions for β-tricalcium phosphate, J. Am. Ceram. Soc. 89 (2006) 688–690, https://doi.org/10.1111/j.1551-2916.2005.00727.x.
[43] S. Kannan, F. Goetz-Neunhoeffer, J. Neubauer, S. Pina, P.M.C. Torres, J.M. F. Ferreira, Synthesis and structural characterization of strontium- and magnesium-co-substituted β-tricalcium phosphate, Acta Biomater. 6 (2010) 571–576, https://doi.org/10.1016/j.actbio.2009.08.009.
[44] S. Kannan, F. Goetz-Neunhoeffer, J. Neubauer, J.M.F. Ferreira, Ionic substitutions in biphasic hydroxyapatite and β-tricalcium phosphate mixtures: structural analysis by rietveld refinement, J. Am. Ceram. Soc. 91 (2008) 1–12, https://doi.org/10.1111/j.1551-2916.2007.02117.x.
[45] T. Kubota, A. Nakamura, K. Toyoura, K. Matsunaga, The effect of chemical potential on the thermodynamic stability of carbonate ions in hydroxyapatite, Acta Biomater. 10 (2014) 3716–3722, https://doi.org/10.1016/j.actbio.2014.05.007.
[46] K. Ohashi, S. Fujiwara, K. Mizuno, Roles of the cytoskeleton, cell adhesion and rho signalling in mechanosensing and mechanotransduction, J. Biochem. 161 (2017) 245–254, https://doi.org/10.1093/jb/mvw082.
[47] C. Ergun, H. Liu, T.J. Webster, E. Olcay, S. Yilmaz, F.C. Sahin, Increased osteoblast adhesion on nanoparticulate calcium phosphates with higher Ca/P ratios, J. Biomed. Mater. Res. A. 85 (2008) 236–241, https://doi.org/10.1002/jbm.a.31555.
[48] H. Pan, B.W. Darvell, Effect of carbonate on hydroxyapatite solubility, Cryst. Growth Des. 10 (2010) 845–850.
[49] D. Nakagawa, M. Nakamura, S. Nagai, M. Aizawa, Fabrications of boron-containing apatite ceramics via ultrasonic spray-pyrolysis route and their responses to immunocytes, J. Mater. Sci. Mater. Med. 31 (2020) 20, https://doi.org/10.1007/s10856-020-6358-z.
[50] O. Gokcekaya, C. Ergun, T.J. Webster, A. Bahadir, K. Ueda, T. Narushima, T. Nakano, Effect of precursor deficiency induced Ca/P ratio on antibacterial and osteoblast adhesion properties of Ag-incorporated hydroxyapatite: reducing Ag toxicity, Materials 14 (2021), https://doi.org/10.3390/ma14123158.